THE JOURNAL OF BIOLOGICAL CHEMISTRY VOL. 284, NO. 3, pp. 1896–1905, January 16, 2009

Hydramacin-1, Structure and Antibacterial Activity of a Protein from the Basal Metazoan *Hydra*[*]

Received for publication, June 20, 2008, and in revised form, November 7, 2008 Published, JBC Papers in Press, November 19, 2008, DOI 10.1074/jbc.M804713200

Sascha Jung[‡], Andrew J. Dingley[§], René Augustin[¶], Friederike Anton-Erxleben[¶], Mareike Stanisak[‖], Christoph Gelhaus[‖], Thomas Gutsmann[**], Malte U. Hammer[**], Rainer Podschun[‡‡], Alexandre M. J. J. Bonvin[§§], Matthias Leippe[‖], Thomas C. G. Bosch[¶], and Joachim Grötzinger[‡1]

From the [‡]Institute of Biochemistry and [‖]Institute of Zoology, Zoophysiology, Christian-Albrechts-University of Kiel, Olshausenstrasse 40, 24098 Kiel, Germany, the [§]Department of Chemistry and School of Biological Sciences, The University of Auckland, Auckland 1142, New Zealand, the [¶]Institute of Zoology, Cell and Developmental Biology, Christian-Albrechts-University of Kiel, Am Botanischen Garten 1-9, 24118 Kiel, Germany, [**]Research Center Borstel, Leibniz-Center for Medicine and Biosciences, Parkallee 10, 23845 Borstel, Germany, the [‡‡]Institute for Infection Medicine, University Hospital Schleswig-Holstein, Campus Kiel, 24105 Kiel, Germany, and the [§§]Bijvoet Center for Biomolecular Research, Science Faculty, Utrecht University, 3584CH, Utrecht, The Netherlands

Hydramacin-1 is a novel antimicrobial protein recently discovered during investigations of the epithelial defense of the ancient metazoan *Hydra*. The amino acid sequence of hydramacin-1 shows no sequence homology to any known antimicrobial proteins. Determination of the solution structure revealed that hydramacin-1 possesses a disulfide bridge-stabilized $\alpha\beta$ motif. This motif is the common scaffold of the knottin protein fold. The structurally closest relatives are the scorpion oxin-like superfamily. Within this superfamily hydramacin-1 establishes a new family of proteins that all share antimicrobial activity.

Hydramacin-1 is potently active against Gram-positive and Gram-negative bacteria including multi-resistant human pathogenic strains. It leads to aggregation of bacteria as an initial step of its bactericidal mechanism. Aggregated cells are connected via electron-dense contacts and adopt a thorn apple-like morphology. Analysis of the hydramacin-1 structure revealed an unusual distribution of amino acid side chains on the surface. A belt of positively charged residues is sandwiched by two hydrophobic areas. Based on this characteristic surface feature and on biophysical analysis of protein-membrane interactions, we propose a model that describes the aggregation effect exhibited by hydramacin-1.

The discovery of bacteria resistant to common classes of antibiotics is rapidly increasing (1). In particular, the rise of multidrug-resistant bacteria is alarming (1). Consequently, there is an urgent need to discover alternative classes of active antibiotic compounds. One such class, which offers tremendous potential, is antimicrobial peptides (AMPs)[2] (2). AMPs act predominantly in a mechanical manner by attacking the microorganisms membranes (3) to form stable or transient pores. Alternatively, AMPs induce micellization in a detergent-like manner (4). Both mechanisms are effective at destroying the target bacteria (5).

Currently, different AMPs have been identified and isolated from a wide variety of organisms including humans, where they mostly participate in the first-line of defense against a pathogen (4). AMPs are grouped into superfamilies and families based on their three-dimensional structures.

Hydramacin-1 is a cationic antimicrobial peptide that was isolated from the basal metazoan *Hydra* and is active against Gram-positive and Gram-negative bacteria (6). The primary structure of hydramacin-1, in particular the location of the cysteine residues in the primary structure, resembles only two cationic antimicrobial peptides isolated from the leech: theromacin (7) and neuromacin (8). The tertiary structures of theromacin and neuromacin are unknown. Furthermore, the mechanism these two peptides use to exhibit their antimicrobial activity is also not entirely understood.

In this study we present the NMR-derived solution structure of hydramacin-1, evaluate the peptide antimicrobial spectrum, and characterize its mode of action using various biophysical techniques. Based on these results, a model of the interrelation between the unusual structural features of hydramacin-1 and its mode of action is presented.

EXPERIMENTAL PROCEDURES

Cloning Procedure—N-terminal sequencing of hydramacin-1 which has been isolated from the pathogen-challenged *Hydra magnipapillata* enabled the isolation of a corresponding cDNA. The nucleic acid sequence was used for alignment analysis with the *Hydra* genome. The identified cDNA was amplified and cloned into the expression vector pET-32a and transformed into the *Escherichia coli* strain BL21 (DE3).

[*] This work was supported by the Deutsche Forschungsgemeinschaft (SFB 617: A1, A9, A17, and A18). The costs of publication of this article were defrayed in part by the payment of page charges. This article must therefore be hereby marked "*advertisement*" in accordance with 18 U.S.C. Section 1734 solely to indicate this fact.

The atomic coordinates and structure factors (code 2k35) have been deposited in the Protein Data Bank, Research Collaboratory for Structural Bioinformatics, Rutgers University, New Brunswick, NJ (http://www.rcsb.org/).

[1] To whom correspondence should be addressed. Tel.: 49-431-880-1686; Fax: 49-431-880-5007; E-mail: jgroetzinger@biochem.uni-kiel.de.

[2] The abbreviations used are: AMPs, antimicrobial peptides; NOE, nuclear Overhauser effect; r.m.s.d., root mean square deviation; MALDI TOF, matrix-assisted laser desorption ionization time-of-flight; MBC, minimal bactericidal concentrations; NBD, 12-(*N*-methyl-*N*-(7-nitrobenz-2-oxa-1,3-diazol-4-yl); HPLC, high performance liquid chromatography; LPS, lipopolysaccharide; *PE*, L-α-phosphatidylethanolamine; PG, L-α-phosphatidyl-DL-glycerol; PI, L-α-phosphatidylinositol; PS, L-α-phosphatidylserine; PC, L-α-phosphatidylcholine; FRET, fluorescence resonance energy transfer; MES, 4-morpholineethanesulfonic acid; SAW, surface acoustic wave.

Expression—Hydramacin-1 was recombinantly expressed in the *E. coli* strain BL21 (DE3) as a fusion protein comprising a thioredoxin-His_6 tag fused with an enterokinase cleavage site N-terminal to the mature protein. Uniformly ^{15}N- and ^{13}C,^{15}N-enriched hydramacin was prepared using M9 minimal medium (9). When cell cultures reached an optical density of ~0.2, isopropyl 1-thio-β-D-galactopyranoside was added to the culture to a final concentration of 1 mM to induce protein expression. The cell growth was continued for 3 h.

Purification, Renaturation, and Cleavage of the Fusion Protein—After expression, bacteria were harvested by centrifugation and resuspended in phosphate-buffered saline containing 0.2% (v/v) Tween 20. The cell suspension was sonicated and centrifuged to isolate the inclusion bodies. The inclusion body pellet was washed twice in phosphate-buffered saline (PBS), 0.2% Tween 20 and 3 times with PBS only. The inclusion body pellet was dissolved in a denaturing buffer (6 M guanidine hydrochloride, 50 mM Tris, pH 7.2) and incubated at 20 °C overnight.

Insoluble material was removed by centrifugation, and the supernatant was incubated at 20 °C for 4 h with Ni^{2+}-NTA-agarose beads (Qiagen, Hilden, Germany) that were equilibrated with the denaturing buffer. After incubation, the beads were thoroughly washed with 6 M guanidine hydrochloride, 50 mM Tris, pH 8.0, buffer before elution of the target protein with the same buffer containing 250 mM imidazole.

The eluted fractions were diluted with denaturation buffer to a final protein concentration of 0.3 mg/ml. This solution was diluted rapidly in a ratio of 1:6 with an aqueous solution containing 4 mM reduced glutathione, 0.4 mM oxidized glutathione. Dilution was achieved by dropping the protein solution slowly (~1 drop/2 s) into the aqueous glutathione containing redox system. Throughout this process the solution was rapidly stirred. After adjustment of the pH to 8.5, the solution was incubated at 20 °C for 72 h. After incubation, the protein sample was concentrated 10-fold with a Vivaspin concentrator (Vivascience AG, Hannover, Germany) and dialyzed against 50 mM Tris, pH 8.0, at 20 °C for 48 h.

The dialyzed protein solution was centrifuged to remove precipitated material. The remaining soluble protein in the supernatant was cleaved by the addition of EnterokinaseMax™ (Invitrogen). Cleavage was performed at 37 °C overnight.

Purification of Mature Hydramacin-1—Purification of mature hydramacin-1 was performed using reversed-phase high performance liquid chromatography (HPLC) on a semi-preparative C18-column (Macherey-Nagel, Düren, Germany). A continuous acetonitrile gradient of 1.4%/min over a time range of 13 min starting at a concentration of 25% (v/v) was used to obtain isolated hydramacin-1. Fractions containing hydramacin-1 were pooled and lyophilized. Purity was confirmed by mass spectrometry in linear mode using a 4700 Proteomics Analyzer MALDI TOF/TOF mass spectrometer (Applied Biosystems, Framingham, MA). Size-exclusion chromatography on a HiLoad Superdex 75 prep grade (16/60) column (Amersham Biosciences) under conditions used for NMR spectroscopy confirmed the monomeric state of the peptide (data not shown).

TABLE 1

Structural statistics for the 20 best structures of hydramacin-1

No distance constraint was violated by more than 0.5 Å in any structure.

Distance restraints	
Intraresidual ($\|i-j\|=0$)	521
Sequential ($\|i-j\|=1$)	179
Medium range ($2 \le \|i-j\| \le 4$)	84
Long range ($\|i-j\| \ge 5$)	262
Hydrogen bonds	20
Disulfide bonds	24
Total	1090
NOE restraint violations	
Mean number of NOE violations >0.3 Å	0.2
Maximum violation	0.46 Å
r.m.s.d. for NOE restraints	0.038 ± 0.013 Å
Deviations from idealized geometry	
Bond lengths	0.0039 ± 0.0002 Å
Bond angles	0.60 ± 0.03°
Impropers	0.48 ± 0.03°
Pairwise r.m.s.d., average r.m.s.d. backbone all	1.25 ± 0.61 Å
Ramachandran plot (for average structure out of 20 structures)	
Most favored regions (%)	60.4%
Additional allowed regions (%)	30.5%
Generously allowed regions (%)	5.6%
Disallowed regions (%)	3.5%

Sample Preparation and NMR Experiments—The freeze-dried ^{15}N- or ^{13}C,^{15}N-enriched peptide was dissolved in a buffer consisting of 50 mM sodium phosphate buffer, pH 5.7, 0.05% NaN_3, and 93% H_2O, 7% D_2O (v/v) and placed into a symmetrical matched microtube (Shigemi, Inc.).

NMR experiments were recorded at 298 K on a Bruker DRX600 spectrometer equipped with 5-mm *z*-gradient ^{13}C,^{1}H,^{15}N cryoprobe optimized for ^{1}H detection. Sequence-specific backbone and side-chain resonance assignments of hydramacin-1 were achieved using the following three-dimensional spectra: HNCA, HNCO, H(CCO)NH, C(CO)NH, HCACO, CBCA(CO)NH, CBCANH, ^{15}N-edited two-dimensional total correlation spectroscopy (TOCSY) and ^{13}C-edited TOCSY. Distance restraints were obtained from three-dimensional ^{15}N-edited and ^{13}C-edited two-dimensional NOE spectroscopy-heteronuclear single quantum correlation experiments recorded with mixing times of 100 and 120 ms, respectively. The long range quantitative-$J_{NC'}$ two H(N)CO experiment was used to identify H-bond scalar couplings (10). Proton chemical shifts were referenced to 3-(trimethylsilyl-propionic acid), whereas ^{15}N and ^{13}C chemical shifts were indirectly referenced (11). The chemical shift data were deposited in the University of Wisconsin Biological Magnetic Resonance Bank database under accession number 15739. All spectra were processed using the program NMRPipe (12). Analysis of the processed spectra was performed with the program NMRview (13).

Structure Calculations—Structure calculations were performed using the program CYANA (14). The calculations were based on 1046 inter-proton distance constraints extracted from the ^{15}N- and ^{13}C-edited two-dimensional NOE spectroscopy spectra. Distances were calibrated so that the median NOE intensity corresponded to a distance of 2.6 Å with a tolerance of 0.125× the bound-squared. Methyl intensities have been divided by 2.0. All lower bounds were set to 1.8 Å. Furthermore, 24 distance restraints between eight cysteine residues generating four disulfide bridges were introduced into the calculations: $2.0 \le d(S_i^{\gamma}, S_j^{\gamma}) \le 2.1$ Å; $3.0 \le d(C_i^{\beta}, S_j^{\gamma}) \le 3.1$ Å; $3.0 \le d(S_i^{\gamma},$

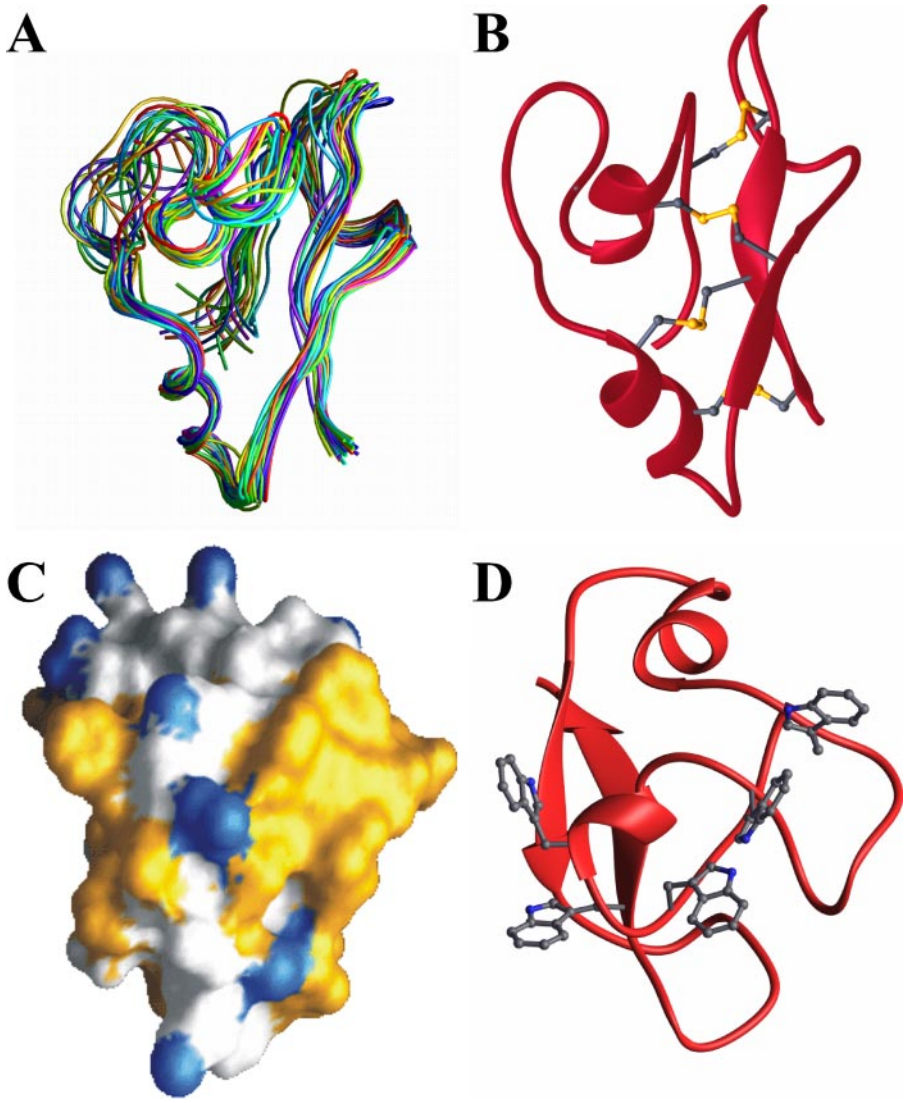

FIGURE 1. **The three-dimensional structure of hydramacin-1.** *A*, spaghetti representation of the superposition of the 20 structures of hydramacin-1. *B*, ribbon representation of the averaged structure of hydramacin-1. Disulfide bridges are depicted in *yellow*, and N and C denote N and C termini, respectively. *C*, molecular surface properties of hydramacin-1. Positive charges of arginine and lysine side chains are colored *blue*, whereas hydrophobic areas are colored *yellow*. *D*, tryptophan side chains are depicted in the structure. The orientation of the structure is the same as in *C*.

C_i^{β}) ≤ 3.1 Å. In addition, 20 distance restraints from 10 hydrogen bonds were set to a range of 1.8–2.0 Å between the donor hydrogen atom and the acceptor oxygen atom and 2.7–3.0 Å between the donor nitrogen atom and the acceptor oxygen atom. Finally, 25 structures with the lowest target functions were selected from 500 calculated structures. The average structure was calculated from the ensemble of these 25 structures and subsequently energy minimized using the GROMOS force field (15). Each of 25 structures of the ensemble was further refined in explicit solvent with an 8 Å water shell using the HADDOCK program (16).

Graphic Representations—All molecular graphical representations were generated using the programs Ribbons (17) and GRASP (18).

Determination of Antimicrobial Activity—The antimicrobial activity of hydramacin-1 was investigated as previously described (19). Briefly, test strains were grown in brain heart infusion broth at 37 °C for 2–3 h. The cells were washed 3 times in 10 mM sodium phosphate buffer, pH 7.4, supplemented with 1% tryptic soy broth, and the cell number was adjusted to 10^4-10^5 cells/ml. From the prepared cell suspension, 100 μl were mixed with 10 μl of hydramacin-1 dissolved in 10 mM sodium phosphate buffer, pH 7.4, and incubated at 37 °C. The final peptide concentrations tested were between 0.0125 and 100 μg/ml. After 2 h of incubation, the colony forming units were determined. For the negative control, bacteria suspensions were supplemented with 10 μl of phosphate buffer, 1% tryptic soy broth. Antimicrobial activity was tested for all strains by determination of LD_{90} (90% lethal dose) or minimal bactericidal concentrations (MBCs) (≥99.9% killing).

Preparation of Liposomes Used for Determination of Membrane Integration by Fluorescence Spectroscopy—Liposomes were prepared essentially as described by Pick (20). Liposomes composed of defined phospholipids were resuspended in 10 mM HEPES, 1 mM EDTA, 150 mM NaCl, pH 7.4, by passing them over a NAP-5 column (Amersham Biosciences). This served as a stock suspension for use in measurements. Except for one, the liposomes used have been generated from lipids purchased from Avanti Polar Lipids Inc. (Alabaster, AL). The lipids are: L-α-phosphatidylethanolamine (PE), L-α-phosphatidyl-DL-glycerol (PG), L-α-phosphatidylinositol (PI), L-α-phosphatidylserine (PS), L-α-phosphatidylcholine (PC), sphingomyelin or asolectin (Fluka, Buchs, Switzerland).

Preparation of Liposomes Used for SAW and FRET Assays—Rough mutant lipopolysaccharide (LPS) from *E. coli* strain WBB01 was extracted by the phenol/chloroform/petroleum ether method (21), purified, lyophilyzed, and transformed into the triethylamine salt form.

Phospholipid liposomes and LPS aggregates were prepared as 1 mM aqueous dispersions of the phospholipids or LPS in three different buffers as follows. The lipids were dissolved in chloroform and the LPS were dissolved in chloroform: methanol (10:1) to a concentration of 1 mg/ml. For the FRET experiments, 1% (mol/mol) of the donor dye NBD PE or of the acceptor dye rhodamine PE) (both were obtained from Molecular Probes, Eugene, OR) was added. The solvent was evaporated under a stream of nitrogen; the lipids were resus-

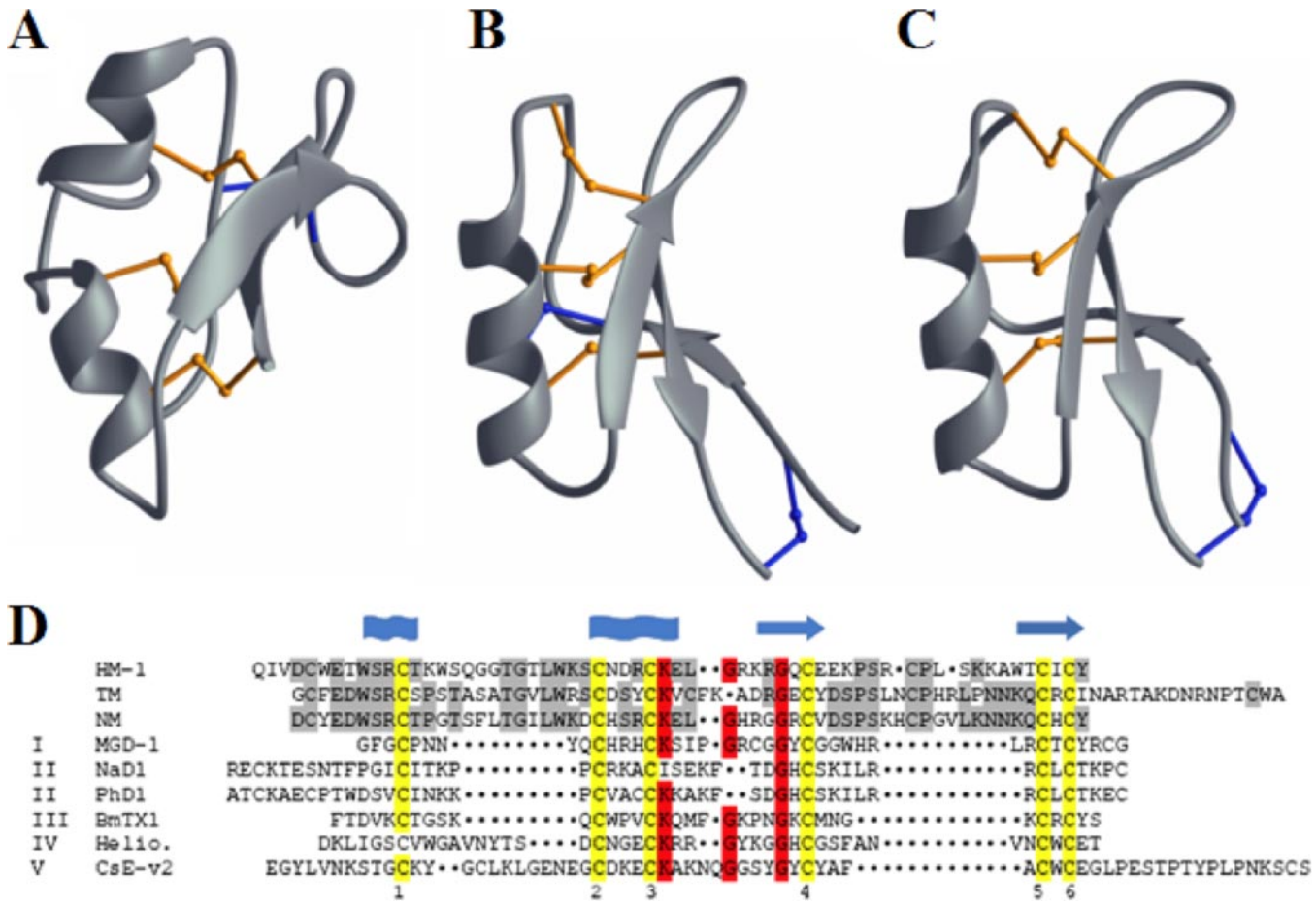

FIGURE 2. **Structural comparison of hydramacin-1, PhD1, and NaD-1 and sequence alignment.** The ribbon representations of the average structures of hydramacin-1 (*A*), *P. hybrida* defensin 1 (*B*), and *N. alata* plant defensin 1 (*C*). Cysteine bridges constituting the knottin-protein fold are depicted in *yellow*, whereas additional disulfide bridges are colored *blue*. *D*, the alignment of hydramacin-1 with representatives of the five families of the scorpion toxin-like superfamily and with theromacin and neuromacin. The alignment is based on the spatially conserved cysteine residues 1–6. *Wavy lines* and *arrows* indicate the positions of α-helices and β-sheets, respectively, in hydramacin-1. Cysteine residues conserved in the tertiary structure are highlighted in *yellow*; other conserved residues are highlighted in *red*. Conserved residues within the macin-protein family are marked in *gray*. *HM-1*, hydramacin-1; *TM*, theromacin (7); *NM*, neuromacin (8); *I*, Mediterranean mussel defensin (*MGD-1*) (32); *II*, *N. alata* plant defensin 1 (*NaD1*) (27); PhD1, *P. hybrida* defensin 1 (26); *III*, *Buthus marten's* toxin 1 (*BmTX1*) (33); *IV*, heliomicin (34); *V*, *Centruroides sculpturatus* Ewing variant 2 toxin (*CsE-v2*) (35).

pended in buffer, mixed thoroughly, and sonicated for 1 min (1 ml solution). Subsequently, the preparation was cooled at 4 °C for 30 min, heated at 56 °C for 30 min, and cooled to 4 °C. Preparations were stored at 4 °C overnight before measurements.

Fluorescence Spectroscopy—Fluorescence experiments were carried out using a F-2500 fluorescence spectrophotometer (Hitachi Ltd., Tokyo, Japan) in the 300–400-nm spectral region at 20 °C. Tryptophan side chains were excited at $\lambda = 280$ nm. The interaction between hydramacin-1 and the different liposome types was measured using 620 μl of a hydramacin-1 solution (20 μg/ml) in 50 mM sodium phosphate with either an acidic pH of 5.7 or a pH of 7.4 and 15 μl of a liposome stock suspension. Spectra were recorded immediately after adding the liposomes. All spectra were measured in triplicate.

SAW Biosensor Assay—To determine the peptide-membrane interaction, the SAW-biosensor system (Biosensor GmbH, Germany) was used. Measurements were performed using a continuous buffer flow of 20 μl/min at 22 °C. By injection of 100 μl of poly-L-lysine (60 μg/ml, Fluka) and the subsequent injection of liposomes or LPS (100 μM), the bilayer was prepared, and finally 100 μl of hydramacin-1 (100 μg/ml in 0.01°% trifluoric acid) was added. All experiments were performed at 22 °C.

FRET-based Fusion Assay—To determine the peptide-induced fusion of lipid liposomes/aggregates of various compositions we used a FRET-based fusion assay. One-half of the respective liposomes were doped with the donor dye NBD PE, and the other half was doped with the acceptor dye rhodamine PE. Mixtures in a ratio of 1:1 of the differently labeled liposomes were prepared with a final concentration of 10 μM. In each experiment, 5 μl of hydramacin-1 (1 mg/ml in 0.01°% trifluoric acid) was added after 50 s. A Fluorolog F1 T11 (Spex Instruments, Edison, NJ) was used to simultaneously measure the fluorescence intensity of the donor and acceptor dyes. All experiments were performed at 37 °C.

Assay for Pore-forming Activity—Pore-forming activity of hydramacin-1 was determined by measuring fluorimetrically the dissipation of a valinomycin-induced membrane potential in liposomes, prepared from soy bean asolectin, as previously described (22). Fluorescence was measured by a fluorescence spectrophotometer (model LS 50B; PerkinElmer

Life Sciences) using excitation and emission wavelengths of 620 and 670 nm, respectively. Pore-forming activity was measured as the initial change in fluorescence intensity over time after the addition of the sample. The pore-forming peptide alamethicin (Sigma-Aldrich) served as a positive control to calibrate the assay.

Assay for Permeabilization of Bacterial Membranes—Bacteria with compromised membranes were detected by monitoring the fluorescence of the DNA binding dye SYTOX Green (Invitrogen) as previously described (23). *Bacillus megaterium* ATCC 14581 in mid-logarithmic phase were washed twice and resuspended in 10 mM HEPES, pH 7.4, containing 25 mM NaCl. A flat-bottom 96-well microtiter plate (Sarstedt, Germany) was coated with 0.1% bovine serum albumin (A2153, Sigma-Aldrich) for 15 min before its use in the assay. Hydramacin-1 was 2-fold serially diluted in 10 mM HEPES, 25 mM NaCl, pH 7.4. Bacteria (1×10^5 colony forming units/50 μl) were incubated with the diluted peptides (25 μl) and 2 μM fluorescent dye SYTOX Green (25 μl in 10 mM HEPES, 25 mM NaCl, pH 7.4) at 20 °C for 1 h. Permeabilization of the bacterial cytoplasmic membrane allows the dye to cross the membrane and to intercalate with the DNA. Excitation of the DNA-bound dye at 495 nm resulted in an increase of emitted fluorescence at 538 nm. Measurements were made in a microtiter plate reader (Fluoroskan II; Labsystems). Membrane-permeabilizing activity of the peptide was expressed as a percentage of permeabilized bacteria. For monitoring the activity at pH 5.2, 20 mM MES and 25 mM NaCl buffer were used. As a control, the antimicrobial peptide cecropin P1 (Sigma-Aldrich) was used. For maximum permeabilization of the bacteria (100% value), cells were incubated with 70% ethanol for 10 min. The values were expressed as the mean of at least two independent experiments, each performed in duplicate.

Electron Microscopy—Bacteria (*E. coli* DH5λ and *Staphylococcus aureus* ATCC 12600) grown to exponential phase were received using the method of Sahly *et al.* (19). Bacteria have been washed twice in 10 mM sodium-phosphate buffer, pH 5.7, and were concentrated to an optical density of 4.6. All further procedures were carried out at 20 °C. The suspension was incubated with hydramacin-1 at final concentrations of 5 or 100 μM peptide. Incubations were performed for 30 min, 1 h, or 2 h. As a negative control, bacteria were incubated with buffer only.

Subsequently, 10% glutaraldehyde (Fluka) in 10 mM sodium phosphate buffer, pH 7.8, was added in a 1:1 ratio to the bacteria suspension and incubated for a further 2 h. Subsequently, samples were washed 3 times in 10 mM sodium phosphate buffer, pH 7.8, and incubated with 3% (w/v) osmium tetroxide in a 10 mM sodium phosphate buffer, pH 7.8, for 1 h. This was followed by 3-fold washing (see above). Afterward samples were treated with non-denatured EtOH at increasing concentrations with an initial concentration of 60% EtOH. Concentrations were subsequently increased in 10% steps until a pure EtOH solution was used. Each incubation step took 15 min. After the EtOH gradient, samples were incubated with 1,2-propylendioxide for at least 5 min before this compound was replaced stepwise by an epoxy resin (agar 100 resin kit, hard, Plano GmbH, Germany).

TABLE 2
Antimicrobial activity of hydramacin-1
LD_{90}, 90% lethal dose; ci, clinical isolate.

Strain	MBC	LD_{90}
	μM	μM
Gram-negative		
Acinetobacter baumannii ATCC 19606	7.1	1.8
Burkholderia cepacia ATCC 25416	>14.3	>14.3
B. cepacia ATCC 17759	>14.3	>14.3
B. cepacia LMG 16654	>14.3	>14.3
C. freundii NCTC 9750	7.1	0.9
C. freundii C7 (ci)	0.9	0.5
E. cloacae Va11263/03 (ci)	>14.3	0.9
E. cloacae Va12270/03 (ci)	0.9	0.5
E. coli ATCC 25922	0.9	0.2
K. pneumoniae ATCC 13883	0.9	0.5
K. oxytoca ATCC 13182	0.9	0.5
Proteus mirabilis ATCC 21100	14.3	0.9
P. vulgaris ATCC 13315	>14.3	3.6
Providencia rettgeri NCTC 7475	>14.3	>14.3
Pseudomonas aeruginosa NCTC 11446	>14.3	14.3
S. typhimurium 10003442 (ci)	0.9	0.5
S. typhimurium 10003630 (ci)	0.9	0.5
Serratia marcescens Mero060/148 (ci)	>14.3	3.6
S. marcescens Mero103/013 (ci)	>14.3	14.3
S. marcescens NCTC 10211	>14.3	1.8
Y. enterocolitca NCTC 11176	0.9	0.2
Multi-resistant Gram-negative		
E. coli Co 86 (ESBL) (ci)	3.6	0.9
K. oxytoca ESBL 33 (ci)	7.1	0.9
K. oxytoca ESBL 37(ci)	3.6	0.9
K. pneumoniae ATCC 700603 (ESBL)	3.6	0.9
Gram-positive		
S. aureus ATCC 6538	>14.3	>14.3
S. hemolyticus ATCC 29970	1.8	0.9
Streptococcus pyogenes ATCC 12344	>14.3	7.1
Multi-resistant Gram-positive		
S. aureus ATCC 33593 (MRSA)	>14.3	>14.3
Enterococcus faecalis ATCC 51299 (VRE)	>14.3	7.1

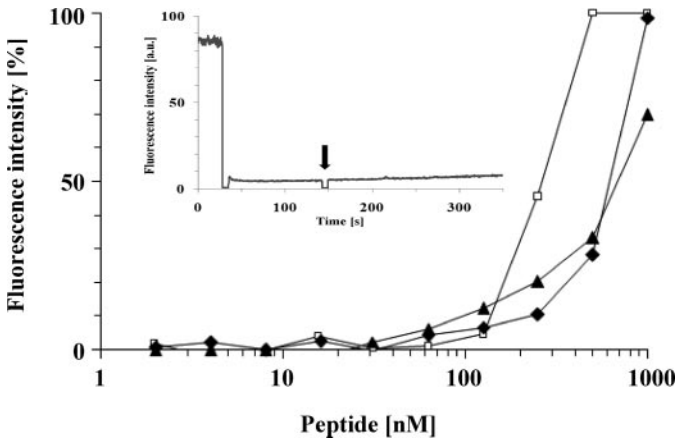

FIGURE 3. **Membrane permeabilization of viable bacteria and pore-forming activity.** Fluorescence of the SYTOX Green dye was used as a measure of bacteria with compromised membranes. Hydramacin-1 permeabilized *B. megaterium* at pH 5.2 (♦) and pH 7.4 (▲). Cecropin P1 at pH 7.4 (□) served as a positive control. *Inset*, measurement of the depolarization of liposomes at pH 5.2 using 0.5 μM hydramacin-1. The result indicates that liposome depolarization as a consequence of pore formation did not occur.

The first step ratio of propylene dioxide to epoxy resin was 2:1 (v/v). In the subsequent steps the ratio was 1:1 and 1:2 before the bacteria samples were finally suspended in epoxy resin only. Suspended samples were incubated overnight. Samples were embedded in fresh epoxy resin and were incubated at 60 °C overnight. From the hardened epoxy resin blocks, ultrathin sections with a thickness of 60 nm were prepared using an ultra-

microtome (Ultracut S, Leica Microsystems GmbH, Germany) equipped with a diamond knife (*histo*, DiS-Galetzka, Germany). These sections were transferred onto copper grids (G2500C, Plano GmbH, Germany) covered with a plastic film (Pioloform-F, Plano GmbH, Germany). Finally, samples were stained with uranyl acetate and lead citrate according to Reynolds (24). Electron micrographs where taken with a TEM 208 S (Philips, Hamburg).

TABLE 3

Fluorescence spectroscopy

The tryptophan fluorescence emission in the absence (base line) and in the presence of liposomes of various compositions at pH 5.7 and 7.4 was measured. Numbers in parentheses display the wavelength shift compared to the base line. All values are in nm.

Liposome type	pH 5.7	pH 7.4
Base line	345.5	343.5
Negatively charged phospholipids		
Phosphatidylglycerol	336.0 (−9.5)	337.5 (−6.0)
Asolectin	338.5 (−7.0)	340.0 (−3.5)
Phosphatidylserine	340.5 (−5.0)	342.5 (−1.0)
Phosphatidylinositol	340.5 (−5.0)	342.5 (−1.0)
Zwitterionic phospholipids		
Sphingomyelin	346.0 (+0.5)	344.5 (+1.0)
Phosphatidylcholine	345.0 (−0.5)	345.0 (+1.5)
Phosphatidylethanolamine	345.5 (0.0)	343.5 (0.0)

RESULTS

Expression and Purification—Hydramacin-1 was recombinantly expressed as an insoluble fusion protein. The inclusion bodies were dissolved under denaturating conditions, and the fusion protein was purified by immobilized metal affinity chromatography and renatured. After proteolytic cleavage to remove the thioredoxine-His_6 tag and carrier protein, mature hydramacin-1 was further purified by reversed-phase HPLC, and its average mass was confirmed to be 7009 Da by MALDI-TOF mass spectrometry.

Tertiary Structure of Hydramacin-1—Structure calculations were performed using 1090 distance restraints (see Table 1). From the 500 calculated structures, the 25 lowest target function structures were selected and subjected to a final water refinement using the HADDOCK software package. An overlay of this ensemble is depicted in Fig. 1*A*. No distance restraint was violated by more than 0.5 Å in any of the 25 structures. The backbone exhibits a root mean square deviation (r.m.s.d.) of 1.13 ± 0.15 Å, whereas the secondary structure elements showed a smaller r.m.s.d. of 0.58 ± 0.12 Å (Table 1). This reflects the well defined secondary structure elements held together by an arrangement of four disulfide bonds and highlights that hydramacin-1 contains unordered regions. The two large loops represent the majority of the unordered regions. The ensemble of 25 structures was used to calculate an average structure (Fig. 1*B*). The molecule possesses two short α-helices (residues 10–14 and 27–33) at the N terminus which are separated by a long flexible loop. The C-terminal region contains two β-strands (residues 38–42 and 56–60) in an antiparallel arrangement separated by a long flexible loop.

Inspection of amino acid side chains contributing to the surface of hydramacin-1 revealed an unusual distribution of arginines and lysines. These residues form a positively charged belt, thereby dividing the molecular surface into two large hydrophobic hemispheres (Fig. 1*C*).

Structural Alignment—Using the solved solution structure of hydramacin-1, a structural similarity search was performed using the Dali server (25). The search led to the identification of only two structures: the *Petunia hybrida* defensin

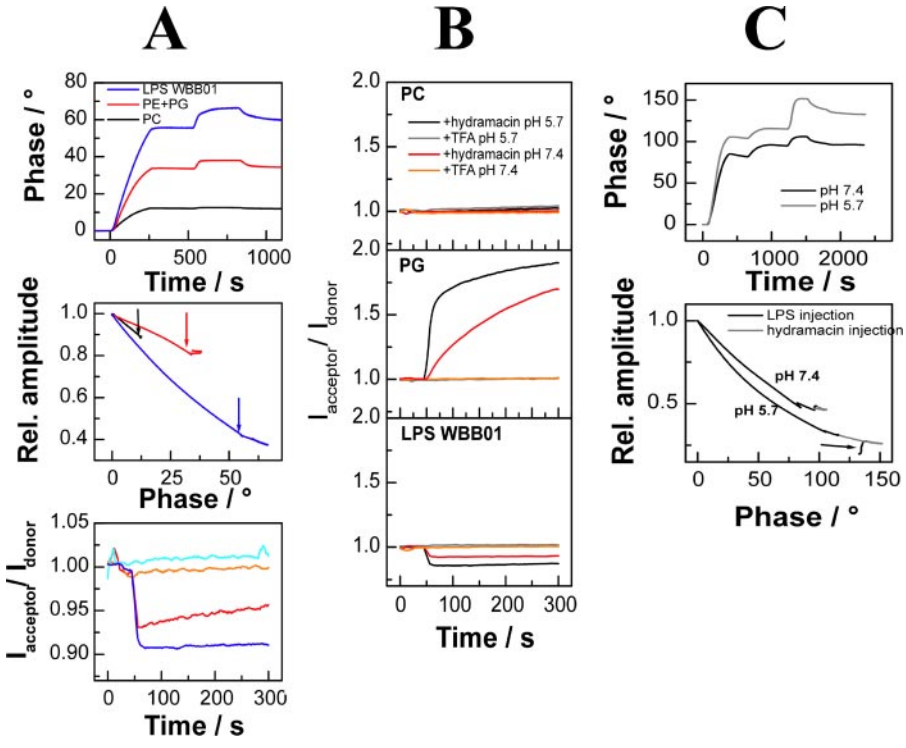

FIGURE 4. **Binding of hydramacin-1 to phospholipids liposomes or LPS aggregates and hydramacin-1-induced fusion.** *A*, *upper* and *middle trace*, SAW experiments demonstrating the influence of the adsorption and desorption of LPS WBB01 aggregates, PG + PE (1:1), or PC liposomes on the phase (time frame 0–500 s) and of hydramacin-1 to the respective matrices (time frame 500–1000 s). *Middle trace*, the traces starting from an amplitude of 1 down to the points marked with the *arrows* show the adsorption and desorption of LPS or the lipids. From the *arrow* onward, the influence of hydramacin-1 can be deduced. *Lower trace*, FRET-based fusion experiments demonstrating intercalation of hydramacin-1 into LPS WBB01 aggregates and PE + PG (1:1) liposomes. The *orange* and *cyan traces* shows the effect of the control (0.01% trifluoric acid). Buffer conditions: 100 mM NaCl, 5 mM HEPES, pH 7. *B*, FRET spectroscopic experiments showing the influence of 5 μl hydramacin-1 (1 mg/ml) on 995 μl of lipid solution (10 μM) (*upper trace*, PC; *middle trace*, PG; *lower trace*, LPS WBB01). Buffer conditions: 50 mM sodium phosphate, pH 5.7 or 7.4 at $T = 37$ °C. 0.01% trifluoric acid (*TFA*) was used as a control. *C*, SAW experiments demonstrating the influence of the pH on the adsorption and desorption of LPS WBB01 aggregates (time frame 0–1200 s), of hydramacin-1 (time frame 1200–1800 s), and of LPS WBB01 aggregates. In the *lower trace* the *black traces* starting from an amplitude of 1 show the adsorption and desorption of LPS. The *gray traces* show the adsorption and desorption of hydramacin-1, and the further *black traces* (*arrow*) show the affect of a subsequent injection of WBB01 LPS. Buffer conditions: 50 mM sodium phosphate, pH 5.7, or 7.4, $T = 22$ °C.

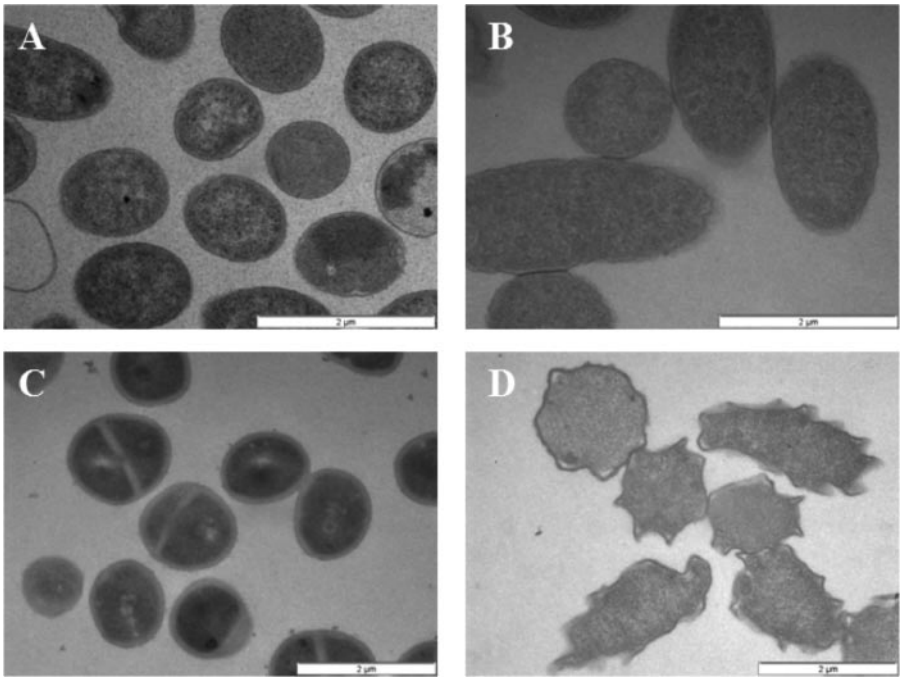

FIGURE 5. **Electron microscopy of hydramacin-1-treated bacteria.** *A*, negative control with buffer (*E. coli*). *B*, 5 μM HM-1 (*E. coli*). *C*, negative control with hydramacin-1 insensitive bacteria (*S. aureus*). *D*, 100 μM HM-1 (*E. coli*).

1 (PhD1, PDB accession code 1n4n) (26) and the *Nicotiana alata* defensin 1 (NaD1, PDB accession code 1mr4) (27). Both proteins belong to the family of plant defensins, which share the knottin fold comprising a disulfide bridge-stabilized $\alpha\beta$ motif. The striking characteristics of the knottin fold are a knot formed by three disulfide bonds and part of the protein backbone in which the disulfide bridge formed by the third and sixth cysteine threads through a macrocycle formed by the first, second, and fifth cysteine and part of the protein backbone (28, 29). The family of plant defensins belongs to the scorpion toxin-like superfamily in the class of small proteins as specified in the Structural Classification of Proteins (SCOP) data base (30). Comparison of the hydramacin-1, PhD1, and NaD1 structures is depicted in Fig. 2, *A–C*. Six of possible eight cysteine residues are in identical spatial positions.

The scorpion toxin-like superfamily consists of five families, namely the long- and short-chain scorpion toxins, the MDG-1 defensin, the insect defensins, and the plant defensins. From each family the first listed member has been chosen for a structural superposition with hydramacin-1 to determine which family hydramacin-1 most closely resembles. To aid this superposition we performed a sequential alignment based on the conserved spatial positions of the cysteine residues constituting the knottin fold (Fig. 2*D*).

In four of the five scorpion toxin-like superfamily members six cysteines are spatially identical and involved in identical cysteine pairings. In the one exception, heliomicin, a single cysteine is located at a different position in space. Nevertheless, we placed the amino acid residues of heliomicin flanking this cysteine according to the conservation of that residue in the primary structures of both peptides. The sequential alignment of hydramacin-1 and its homologues theromacin and neuromacin (Fig. 2*D*) clearly showed that these proteins constitute a new family within the scorpion toxin-like superfamily, which we have named the macin family.

Antimicrobial Activity of Hydramacin-1—To test the antimicrobial activity of hydramacin-1 against microbes, we used a wide range of human Gram-negative and Gram-positive pathogens in a broth-microdilution assay. Hydramacin-1 revealed the highest activities against the Gram-negative species *Citrobacter freundii* (C7), *Enterobacter cloacae* (Va12270/03), *E. coli*, *Klebsiella pneumoniae* and *Klebsiella oxytoca*, *Salmonella typhimurium*, and *Yersinia enterolitca* (Table 2). In each case, very low peptide concentrations of less than 1 μM were sufficient to kill all (99.9%) of these bacteria. The highest killing activity against Gram-positive pathogens was observed for *Staphylococcus hemolyticus*, for which the peptide concentration needed for total killing was 1.8 μM. Hydramacin-1 was effective at killing most of the tested multi-resistant strains, albeit at higher concentrations.

Membrane Permeabilization—Membrane permeabilization assays were performed to determine the mechanism by which hydramacin-1 kills microbes. The results showed that hydramacin-1 is able to permeabilize membranes of viable bacteria at low and neutral pH values (Fig. 3). To further characterize the peptide mode of action, its potential pore-forming activity was investigated by using a minimalistic membrane system consisting of multilamellar liposomes prepared from asolectin, a crude phospholipids mixture of soy bean, and by monitoring the liposome depolarization induced by hydramacin-1. Under the conditions used, pore-forming activity was not detectable (Fig. 3 *inset*).

Fluorescence Spectroscopy—The five tryptophans of hydramacin-1 are all solvent-exposed (Fig. 1*D*), indicating that these residues are likely to play a key role in the interaction with and insertion into the target membrane. To examine whether hydramacin-1 is able to insert into the hydrophobic environment of liposomes via the tryptophan residues, fluorescence spectroscopy was used. We tested negatively and neutrally charged liposomes prepared from various types of phospholipids at pH values of 5.7 and 7.4. Table 3 summarizes the results obtained by fluorescence spectroscopy.

A shift of wavelength of the fluorescence emission maximum was observed with negatively charged liposomes only. The strongest shift to a shorter wavelength (9.5 nm) was observed with PG liposomes at pH 5.7. This is indicative of tryptophan residues interacting with the membrane bilayer. Liposomes consisting of asolectin exhibited a slightly smaller shift (7.0 nm). PS and PI liposomes resulted in a shift of 5.0 nm. Zwitterionic liposomes prepared from PC, PE, and sphingomyelin did not

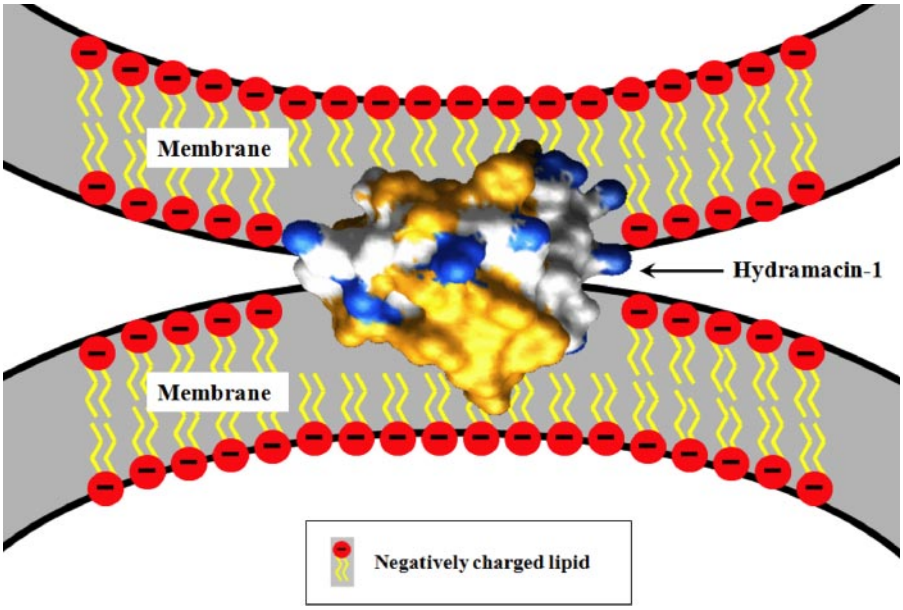

FIGURE 6. **Model of the mode of action of hydramacin-1.** Schematic representation of two negatively charged membranes sandwiching hydramacin-1. Hydrophobic amino acid residues contributing to the molecular surface of hydramacin-1 are colored *yellow*, whereas cationic surface areas are colored *blue*.

induce a significant shift of the fluorescence emission maximum, indicating that the tryptophan residues were not in contact with the lipid bilayer. A similar situation was observed at pH 7.4 but with smaller shifts when PS and PI were used. This indicates that hydramacin-1 preferentially interacts with negatively charged membrane constituents, such as PG. During experiments we observed the formation of precipitates consisting of hydramacin-1-lipid complexes. To assess whether the precipitates are formed due to fusion of liposomes, SAW and FRET assays were carried out.

SAW Biosensor Experiments and FRET Assays—The phase/time as well as the amplitude/phase diagram (Fig. 4*A*, *upper* and *middle trace*) is in agreement with the results from the tryptophan-fluorescence experiments; there is no interaction between hydramacin-1 and PC. In contrast, PE + PG and LPS matrices led to similar adsorption of the peptide as observed by the increase of the phase. The amplitude, which depends to a first approximation on the viscoelastic properties of the material adsorbed on the sensor surface, was only influenced in the case of LPS membranes. These results indicate that a stronger interaction exists between LPS and hydramacin-1 compared with the interaction between PE + PG and hydramacin-1. Using the same buffer system, a FRET-based fusion assay was performed. The results show that hydramacin-1 does not induce the fusion of LPS aggregates or PE + PG liposomes (Fig. 4*A*, *lower trace*).

To further investigate the influence of the lipid matrix and pH of the buffer on the fusion of liposomes and LPS aggregates, we used buffers containing 50 mM sodium phosphate, pH 5.7 and 7.4. At both pH values no interaction between hydramacin-1 and PC liposomes was observed (Fig. 4*B*, *upper trace*). In the case of pure PG liposomes, the FRET signal increased at both pH values. This is indicative for a peptide-induced fusion (Fig. 4*B*, *middle trace*). The interaction was stronger and in particular faster at the lower pH. Hydramacin-1 induced no fusion of LPS aggregates, but the peptide intercalates into the LPS membranes at both pH values; however, the interaction at pH 7.4 was significant weaker (Fig. 4*B*, *lower trace*). The FRET assay does not allow a distinction between an intercalation of the peptide without any further effects and an intercalation with subsequent aggregation of the LPS aggregates. Therefore, we used the SAW biosensor experiments at pH 5.7 and 7.4 in which we first injected LPS WBB01 aggregates two times, in a second step injected hydramacin-1, and in a third step injected LPS WBB01 aggregates once again. Fig. 4*C* shows that at low pH hydramacin-1 bound stronger to the LPS membranes (Fig. 4*C*, *upper trace*) and that the subsequent injection of LPS aggregates led to a change of the amplitude (Fig. 4*C*, *lower trace*). This result is indicative for a hydramacin-1-induced interaction between two LPS matrices at pH 5.7 but not at pH 7.4.

Electron Microscopy of Hydramacin-1-treated Bacteria—Incubation of *E. coli* DH5λ with hydramacin-1 at 5 μM led to the formation of electron-dense contacts between the cells that were not observed with control bacteria treated with buffer only (Fig. 5, *A* and *B*). The peptide concentration tested was 10^3–10^4 times less than the MBCs determined. The incubation of the peptide at 20× higher concentration (which is closer to the MBC values) showed that the bacteria retained the cell-cell contacts, but in addition the cells had changed their morphology to a thorn apple-like shape (Fig. 5*C*). *S. aureus* bacteria, which had been insensitive to hydramacin-1 under the conditions tested to determine the MBC, were used as the negative control. These bacteria did not show cell-cell contacts at a concentration of 5 μM hydramacin-1 (Fig. 5*D*). No differences were observed between the three incubation periods tested.

DISCUSSION

The solution structure of the antibacterial protein hydramacin-1 from the basal metazoan *H. magnipapillata* reveals a disulfide bridge-stabilized αβ motive that is the common scaffold of the knottin-protein fold that was first described by Rees and Lipscomb (28). SCOP (30) places hydramacin-1 as a member of the scorpion toxin-like superfamily which is further subdivided into five families. Comparison of several members of all five families of the scorpion toxin-like superfamily suggests that hydramacin-1 represents the first member of a new family within the scorpion toxin-like superfamily. Comparison of the hydramacin-1 structure with all 103 structures of the members of the scorpion toxin-like superfamily that are listed in the SCOP data base (30) revealed that, except for one, none of these structures contains an additional α-helix at the N terminus. The one exception is the scorpion toxin Bj-xtrIT (accession

code 1bcg) which belongs to the long-chain scorpion toxins. This additional N-terminal helix can also be described as one long α-helix (Figs. 1*B* and 2*A*) that is interrupted by a loop containing three glycine residues. The glycine residues confer flexibility to this region. Because this loop consists of primarily hydrophobic residues, this region may represent an important interaction site with target membrane moieties. Compared with hydramacin-1, none of the listed proteins have long flexible loops separating the typical secondary structure elements of the knottin fold. In addition, hydramacin-1 is derived from *Hydra*, which is an organism of ancient origin compared with scorpions, spiders, insects, plants, or mussels. Moreover, hydramacin-1 exhibits a high degree of sequence identity to two other antimicrobial peptides isolated from leech: theromacin and neuromacin (7, 8). This observation points to two additional members of this new family, which we have termed the macins.

Here, we demonstrate that hydramacin-1 is active against a broad range of microbes including some clinical isolates of *Enterobacter cloacae* and multi-resistant *K. oxytoca.* This makes hydramacin-1 a promising template for a new class of antibiotics.

Hydramacin-1 promotes aggregation of bacteria at significantly lower concentrations relative to the amount of bacteria present as compared with the MBCs found. Therefore, this cell aggregation effect occurs before the extensive killing effects of the peptide and may represent the initial step of the peptide killing mechanism. Bacteria exposed to hydramacin-1 form electron-dense contacts and change their cell morphology to a thorn apple-like shape. Because of the double-amphipathic character of hydramacin-1 represented by the two hydrophobic hemispheres sandwiched by a belt of positive charges, we suggest a model that explains the observed aggregation of bacteria in the presence of hydramacin-1 (Fig. 6). The two hydrophobic patches of the peptide immerse into the outer leaflets of the membranes of two individual bacterial cells. Thereby, negative charges of the phospholipids of the membrane surfaces, which would probably decrease the possible spontaneous aggregation of individual bacterial cells, are compensated by the band of positive charges surrounding the molecule at the immersion point. Therefore, the peptide-lipid complex is stabilized by hydrophobic as well as electrostatic forces. However, peptide-lipid interactions might be initiated mainly by attraction of opposite charges because the immersion of hydramacin-1 into the membrane as well as the fusion or precipitation effect of liposomes and LPS aggregates is highly affected by pH.

The phenomenon of aggregation was observed with liposomes as well. As these model membranes consist of only lipids, the aggregation must be a result exclusively of peptide-lipid and peptide-charge interactions. Consequently, one can exclude receptor mediation.

Enforced proximity of cells might lead to fusion as observed with model membranes from liposomes. However, fused cells have not been observed, and the absence of such an observation may be a consequence of the higher complexity of the bacterial membrane compared with liposomes.

Explanations for the observed change in cell morphology are currently suggestive. The results clearly showed that hydramacin-1 permeabilizes the bacterial membrane. Consequently, hydramacin-1 may invade the cells and affect intracellular secondary targets like the cytoskeleton (31), leading to the observed change in morphology. Interference with the polymerization or depolymerization of filaments might lead to invaginations or formation of protuberances of the bacterial membrane as observed. However, further investigations are required to better understand the molecular details of these secondary events after the initial aggregation/permeabilization of cells.

Acknowledgments—We thank Sonja Hollmer, Christine Hamann, Antje Thomas, and Silvia Voss for excellent technical assistance and Matthias Michalek for preparing the liposomes.

REFERENCES

1. Alanis, A. J. (2005) *Arch. Med. Res.* **36,** 697–705
2. Marshall, S. H., and Arenas, G. (2003) *Electronic Journal of Biotechnology* (*online*) **6,** 271–284
3. Zasloff, M. (2002) *Nature* **415,** 389–395
4. Jenssen, H., Hamill, P., and Hancock, R. E. (2006) *Clin. Microbiol. Rev.* **19,** 491–511
5. Gallo, R. L., Murakami, M., Ohtake, T., and Zaiou, M. (2002) *J. Allergy Clin. Immunol.* **110,** 823–831
6. Bosch, T. C. G., Augustin, R., Anton-Erxleben, F., Fraune, S., Hemmrich, G., Zill, H., Rosenstiel, P., Jacobs, G., Schreiber, S., Leippe, M., Stanisak, M., Grötzinger, J., Jung, S., Podschun, R., Bartels, J., Harder, J., and Schröder, J. M. (2008) *Dev. Comp. Immunol.*, in press
7. Tasiemski, A., Vandenbulcke, F., Mitta, G., Lemoine, J., Lefebvre, C., Sautiere, P. E., and Salzet, M. (2004) *J. Biol. Chem.* **279,** 30973–30982
8. Schikorski, D., Cuvillier-Hot, V., Leippe, M., Boidin-Wichlacz, C., Slomianny, C., Macagno, E., Salzet, M., and Tasiemski, A. (2008) *J. Immunol.* **181,** 1083–1095
9. Dingley, A. J., Lorenzen, I., and Grotzinger, J. (2008) *Methods Mol. Biol.* **451,** 441–462
10. Cordier, F., and Grzesiek, S. (1999) *J. Am. Chem. Soc.* **121,** 1601–1602
11. Markley, J. L., Bax, A., Arata, Y., Hilbers, C. W., Kaptein, R., Sykes, B. D., Wright, P. E., and Wuthrich, K. (1998) *J. Biomol. NMR* **12,** 1–23
12. Delaglio, F., Grzesiek, S., Vuister, G. W., Zhu, G., Pfeifer, J., and Bax, A. (1995) *J. Biomol. NMR* **6,** 277–293
13. Johnson, B. A. (2004) *Methods Mol. Biol.* **278,** 313–352
14. Guntert, P. (2004) *Methods Mol. Biol.* **278,** 353–378
15. van Gunsteren, W. F., Billeter, S. R., Eising, A. A., Hünenberger, P. H., Krüger, P., Mark, A. E., Scott, W. R. P., and Tironi, I. G. (1996) *Biomolecular Simulation: The GROMOS96 Manual and User Guide*, vdf Hochschulverlag AG, Zürich
16. Dominguez, C., Boelens, R., and Bonvin, A. M. J. J. (2003) *J. Am. Chem. Soc* **125,** 1731–1737
17. Carson, M. (1991) *J. Appl. Crystallogr.* **24,** 946–950
18. Nicholls, A., Sharp, K. A., and Honig, B. (1991) *Proteins* **11,** 281–296
19. Sahly, H., Schubert, S., Harder, J., Rautenberg, P., Ullmann, U., Schroder, J., and Podschun, R. (2003) *Antimicrob. Agents Chemother.* **47,** 1739–1741
20. Pick, U. (1981) *Arch Biochem. Biophys.* **212,** 186–194
21. Galanos, C., Luderitz, O., and Westphal, O. (1969) *Eur. J. Biochem.* **9,** 245–249
22. Leippe, M., Ebel, S., Schoenberger, O. L., Horstmann, R. D., and Muller-Eberhard, H. J. (1991) *Proc. Natl. Acad. Sci. U. S. A.* **88,** 7659–7663
23. Herbst, R., Ott, C., Jacobs, T., Marti, T., Marciano-Cabral, F., and Leippe, M. (2002) *J. Biol. Chem.* **277,** 22353–22360
24. Reynolds, E. S. (1963) *J. Cell Biol.* **17,** 208–212
25. Holm, L., and Sander, C. (1996) *Science* **273,** 595–603
26. Janssen, B. J., Schirra, H. J., Lay, F. T., Anderson, M. A., and Craik, D. J. (2003) *Biochemistry* **42,** 8214–8222

27. Lay, F. T., Schirra, H. J., Scanlon, M. J., Anderson, M. A., and Craik, D. J. (2003) *J. Mol. Biol.* **325,** 175–188
28. Rees, D. C., and Lipscomb, W. N. (1982) *J. Mol. Biol.* **160,** 475–498
29. Le Nguyen, D., Heitz, A., Chiche, L., Castro, B., Boigegrain, R. A., Favel, A., and Coletti-Previero, M. A. (1990) *Biochimie* (*Paris*) **72,** 431–435
30. Murzin, A. G., Brenner, S. E., Hubbard, T., and Chothia, C. (1995) *J. Mol. Biol.* **247,** 536–540
31. Errington, J. (2003) *Nat. Cell Biol.* **5,** 175–178
32. Yang, Y. S., Mitta, G., Chavanieu, A., Calas, B., Sanchez, J. F., Roch, P., and Aumelas, A. (2000) *Biochemistry* **39,** 14436–14447
33. Blanc, E., Romi-Lebrun, R., Bornet, O., Nakajima, T., and Darbon, H. (1998) *Biochemistry* **37,** 12412–12418
34. Lamberty, M., Caille, A., Landon, C., Tassin-Moindrot, S., Hetru, C., Bulet, P., and Vovelle, F. (2001) *Biochemistry* **40,** 11995–12003
35. Cook, W. J., Zell, A., Watt, D. D., and Ealick, S. E. (2002) *Protein Sci.* **11,** 479–486